













GaN-on-diamond technology platform: Bonding-free membrane manufacturing process

Cite as: AIP Advances **10**, 035306 (2020); <https://doi.org/10.1063/1.5129229>

Submitted: 13 January 2020 . Accepted: 10 February 2020 . Published Online: 03 March 2020

Matthew D. Smith , Jerome A. Cuenca , Daniel E. Field, Yen-chun Fu, Chao Yuan , Fabien Massabuau , Soumen Mandal , James W. Pomeroy , Rachel A. Oliver , Michael J. Uren , Khaled Elgaid , Oliver A. Williams , Iain Thayne , and Martin Kuball 



View Online



Export Citation



CrossMark

AVS Quantum Science

Co-Published by



RECEIVE THE LATEST UPDATES

AIP
Publishing

GaN-on-diamond technology platform: Bonding-free membrane manufacturing process

Cite as: AIP Advances 10, 035306 (2020); doi: 10.1063/1.5129229

Submitted: 13 January 2020 • Accepted: 10 February 2020 •

Published Online: 3 March 2020



View Online



Export Citation



CrossMark

Matthew D. Smith,¹ Jerome A. Cuenca,² Daniel E. Field,³ Yen-chun Fu,¹ Chao Yuan,³ Fabien Massabuau,⁴ Soumen Mandal,² James W. Pomeroy,³ Rachel A. Oliver,⁴ Michael J. Uren,³ Khaled Elgaid,² Oliver A. Williams,² Iain Thayne,¹ and Martin Kuball^{3,a)}

AFFILIATIONS

¹School of Engineering, University of Glasgow, Glasgow G12 8LT, United Kingdom

²School of Engineering, Cardiff University, Cardiff CF24 3AA, United Kingdom

³Center for Device Thermography and Reliability (CDTR), H. H. Wills Physics Laboratory, University of Bristol, Bristol BS8 1TL, United Kingdom

⁴Department of Materials Science and Metallurgy, University of Cambridge, 27 Charles Babbage Road, Cambridge CB3 0FS, United Kingdom

^{a)} Author to whom correspondence should be addressed: Martin.Kuball@bristol.ac.uk

ABSTRACT

GaN-on-diamond samples were demonstrated using a membrane-based technology. This was achieved by selective area Si substrate removal of areas of up to 1 cm × 1 cm from a GaN-on-Si wafer, followed by direct growth of a polycrystalline diamond using microwave plasma chemical vapor deposition on etch exposed N-polar AlN epitaxial nucleation layers. Atomic force microscopy and transmission electron microscopy were used to confirm the formation of high quality, void-free AlN/diamond interfaces. The bond between the III-nitride layers and the diamond was validated by strain measurements of the GaN buffer layer. Demonstration of this technology platform is an important step forward for the creation of next generation high power electronic devices.

© 2020 Author(s). All article content, except where otherwise noted, is licensed under a Creative Commons Attribution (CC BY) license (<http://creativecommons.org/licenses/by/4.0/>). <https://doi.org/10.1063/1.5129229>

Transistors created on a GaN-on-diamond material system have attracted significant interest in recent years due to their increased high frequency and high power handling potential when compared to commercially established GaN-on-SiC technologies. The high thermal conductivity of polycrystalline diamond substrates significantly improves thermal transistor management, increasing by up to ~3× the power density handling capability of GaN-based radio-frequency (RF) devices.¹ This performance benefit can be utilized to increase RF transmitter output power as required for next generation (5G and beyond) wireless communication systems with enhanced reliability. The current GaN-on-diamond state-of-the-art fabrication process uses amorphous dielectric interlayers as seed layers for diamond growth,^{1–6} following wafer bonding to a temporary carrier wafer^{4,7–9} and additional processing. The inclusion of a wafer bonding stage

increases manufacturing complexity and potentially compromises the device surface, negatively impacting device performance.

In this work, we describe a membrane-based GaN-on-diamond production methodology which obviates the need for bonding to a carrier wafer. A polycrystalline diamond is deposited directly on membranes formed from GaN-on-Si wafers by selective area substrate removal, enabling the growth of a 50 μm thick crack-free diamond directly on the exposed back-side (N-polar face) of AlN epitaxial nucleation layers. The simplified production method provides a route to GaN-on-diamond devices and circuits with improved performance and manufacturability.

AlGaIn/GaN heterostructures were grown by metalorganic chemical vapor deposition on 1 mm thick Si substrates of a diameter of 150 mm. High quality GaN growth is initiated via an AlN nucleation layer (200 nm), followed by AlGaIn strain relief layers

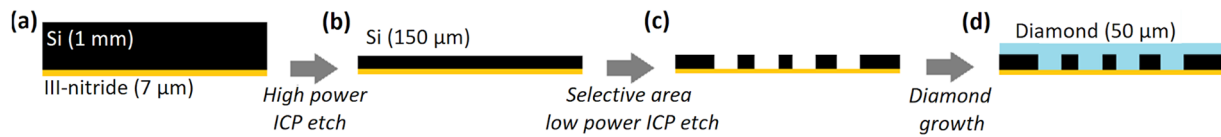


FIG. 1. Process schematic showing (a) GaN-on-Si sample, (b) substrate thinning by plasma etching, (c) formation of III-nitride membranes by plasma etching, and (d) GaN-on-diamond membranes.

($\sim 5 \mu\text{m}$) that are used to manage the stress occurring due to differences in the coefficients of thermal expansion between Si and III-nitride layers during growth cooldown.¹⁰ A 1.5 μm thick GaN buffer layer, the lower 1 μm of which was C-doped, was grown above the AlGaIn strain relief layers. This was capped with an $\text{Al}_{0.2}\text{Ga}_{0.8}\text{N}$ barrier (20 nm) and a GaN surface layer (3 nm). Wafers were scribed using a mechanical saw to produce 12 mm \times 12 mm square samples and then subjected to a high power (900 W) inductively-coupled plasma (ICP) $\text{SF}_6/\text{C}_4\text{F}_8$ modified Bosch etch process,¹¹ thinning the Si substrate to 150 μm . A reduced power (600 W) ICP $\text{SF}_6/\text{C}_4\text{F}_8$ Bosch etch was used to remove the remaining Si substrate in selected areas (defined using photolithography), with *in situ* end-point interferometry employed to determine the etch duration. This process, depicted in Fig. 1, results in III-nitride membranes surrounded by Si supports. The etch exposed N-polar AlN membrane surfaces were imaged using atomic force microscopy (AFM).

Diamond growth was achieved using a Carat systems CTS6U microwave plasma chemical vapor deposition (MPCVD) reactor. Prior to growth, a modified diamond-on-AlN seeding process was used, similar to that found in Ref. 12. The exposed III-nitride membranes were first pre-treated in a N_2/H_2 microwave plasma with a forward power of 1.5 kW at 20 Torr. A nano-diamond colloid solution was then pipetted onto the substrates, which were rinsed carefully in de-ionized water and dried on a hotplate for 10 min at 115 $^\circ\text{C}$. After seeding, diamond growth was achieved in a CH_4/H_2 microwave plasma with a power of 5.0–5.5 kW at 110–120 Torr and a CH_4 concentration of 3% in a 500 sccm flow rate. Under these conditions, with a typical growth rate of approximately 2–3 $\mu\text{m}/\text{h}$, growth runs were conducted for at least 24 h to ensure a diamond thickness of over 50 μm . The temperature of the sample during growth was monitored using a Williamson dual wavelength pyrometer. The samples were then cleaned using organic solvents to remove carbon contamination deposited during diamond growth.

The interface between the diamond and AlN was imaged using scanning transmission electron microscopy (STEM). The sample was lifted out of the membrane region from the III-nitride face using an FEI Helios Nanolab focused ion beam (FIB), and high-angle annular dark field STEM (HAADF-STEM) images were taken on an FEI Osiris microscope operated at 200 kV. Raman spectroscopy was carried out on both the III-nitride surface and the diamond using a Renishaw InVia system with a 488 nm laser excitation source.

Figure 2 shows III-nitride membrane samples prior to diamond growth. A range of circular and squared membranes of varying sizes were produced, from 1 cm \times 1 cm squares [Fig. 2(b)] to 0.5 mm diameter circles [Fig. 2(c)], with the former representing

an aspect ratio of $\sim 10^3$ considering a total III-nitride layer thickness of $\sim 7 \mu\text{m}$. The ICP power reduction during the etching steps of the Bosch processes described above was found to be essential to prevent cracking of the membranes. Complete removal of the Si substrate was verified by a characteristic increase in surface reflectivity, as monitored by *in situ* interferometry, and the high optical reflectivity of the exposed III-nitride surfaces relative to the remaining Si support structure enabled rapid visual inspection. The exposed N-polar AlN nucleation layer surfaces had an rms roughness of 0.9 nm over a 2 $\mu\text{m} \times 2 \mu\text{m}$ area, as measured by AFM, illustrated in Fig. 2(d). The surface morphology and roughness are comparable to recent studies exploring N-polar AlN for optoelectronics applications.¹³

Figures 3(a) and 3(b) show the membrane sample from Fig. 2(a) during and after diamond growth, respectively, with no noticeable macro-scale deformation. Diamond growth temperature as measured using *in situ* pyrometry varied between 700 $^\circ\text{C}$ and 800 $^\circ\text{C}$ although this method only provides a spot measurement on the sample and some inhomogeneity in the diamond is apparent from Fig. 3(b). This is attributed to the elliptical plasma density profile and electric field focusing around the sample corners, causing an increase in temperature and difference in growth conditions. Raman spectroscopy was used to quantify the quality and stress in the diamond across the sample. The diamond sp^3 peak was observed at an

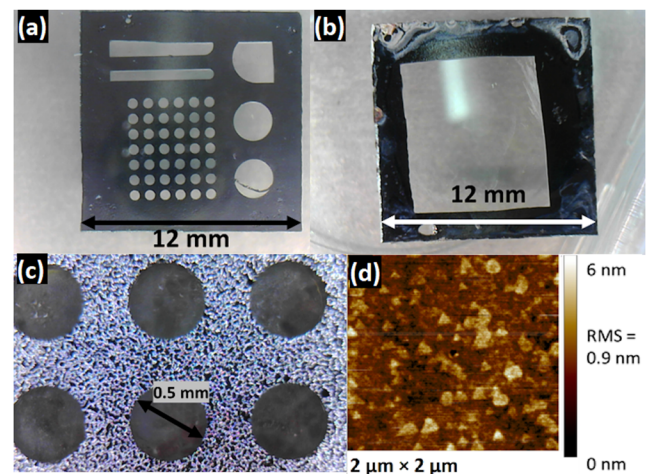


FIG. 2. (a) Multiple GaN-on-Si membranes on a single sample, (b) the large area membrane with an aspect ratio of $\sim 10^3$, (c) the optical microscope image (5 \times) of III-nitride membranes with exposed N-polar AlN surfaces, and (d) the AFM image of the N-polar AlN surface.

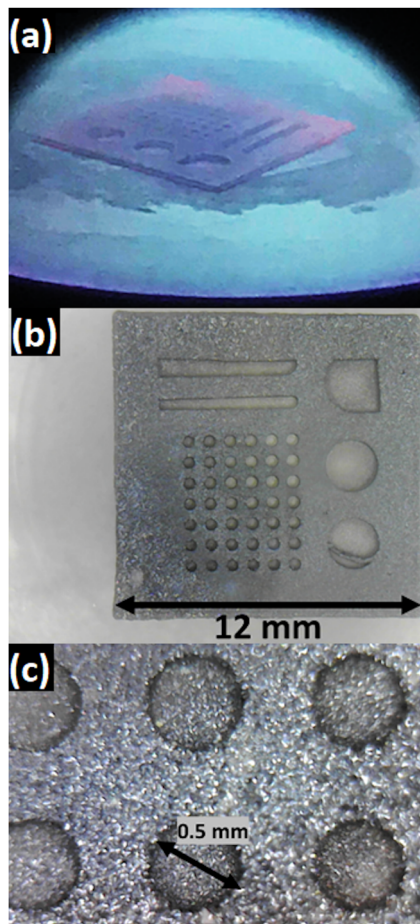


FIG. 3. Membrane samples (a) during and (b) after diamond growth and (c) the optical microscope image (5 \times) of membranes after diamond growth.

average position of $1332 \text{ cm}^{-1} \pm 0.3 \text{ cm}^{-1}$ with an average full width half maximum (FWHM) of $6.0 \text{ cm}^{-1} \pm 1.0 \text{ cm}^{-1}$. These numbers correspond to a diamond with a good crystal quality and negligible stress.¹⁴ We note that Raman measurements made at points which

were glowing red in Fig. 3(a), i.e., near the edges of the sample, had an increased FWHM ($7.2 \text{ cm}^{-1} \pm 1.0 \text{ cm}^{-1}$) compared to the other regions ($5.3 \text{ cm}^{-1} \pm 1.0 \text{ cm}^{-1}$), indicative of diamond regions with a lower crystal quality and a higher defect density; now, we concentrate on the central regions of the sample. For the 0.5 mm diameter membranes, located in the central region of the sample, Fig. 3(c) shows that a continuous diamond layer has been deposited across both the III-nitride membrane and the Si border. In contrast, for the sample with a larger 1 cm \times 1 cm square membrane, the thermal stresses induced when cooling from the growth temperature to room temperature resulted in III-nitride membrane fracturing along the hexagonal crystal planes. This is attributed to a mismatch in the coefficient of thermal expansion and elastic moduli of the III-nitride stack, the silicon frame, and the diamond. Since the thermal expansion coefficient of the diamond is much lower than that of the layers in the III-nitride stack, upon cooling, the III-nitride layers are held in tension, and the membrane shatters if local stress values exceed the tensile yield strength. The actual practical limitations on membrane dimensions require further investigation, and it is suspected that rounded edges may mitigate local stress exceeding mechanical yield values.¹⁵

For 0.5 mm diameter circular membranes [Fig. 3(c)], Raman spectroscopy measurements [Fig. 4(a)] confirmed the presence of tensile, biaxial stress in the GaN buffer layers in every membrane measured, reaching a maximum of 1 GPa at the edges of the membranes [Fig. 4(b)]. The standard relationship between the stress induced Raman peak shift and biaxial stress is used,¹⁶ with reference to the relaxed GaN E_2 phonon frequency value of 567.2 cm^{-1} .¹⁷ The final stress in the GaN film depends on the in-built stress at the diamond deposition temperature and geometric effects such as bowing, buckling, and clamping at the rim of the membrane, which has a non-trivial solution. To determine an approximated thermomechanical stress, we can assume a flat membrane and uniform biaxial stress and apply the equation $\Delta\sigma = E \cdot \Delta\alpha \cdot \Delta T / (1 - \nu)$, where $\Delta\sigma$ is the change in stress, $E = 295 \text{ GPa}$ ¹⁸ and $\nu = 0.35$ are the Young's modulus and Poisson ratio of GaN, respectively, and $\Delta\alpha = 1.85 \times 10^{-6} \text{ K}^{-1}$ is the average difference in the thermal expansion coefficient between the GaN film¹⁹ and diamond²⁰ over the temperature range $\Delta T = 800 \text{ }^\circ\text{C}$, i.e., subtracting the ambient temperature from the diamond deposition temperature. A biaxial tensile stress value of $\sim 0.7 \text{ GPa}$ was determined using this

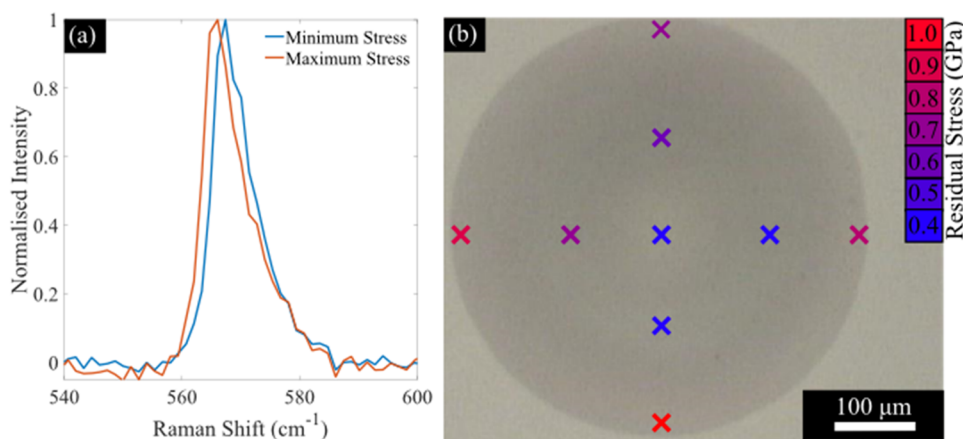


FIG. 4. (a) Raman spectra taken at the center (0.4 GPa, blue line) and the bottom (1 GPa, red line) of the membrane and (b) the variation in stress across a membrane. A maximum error of 10% for these values was estimated from the fitting error using the bootstrap method.

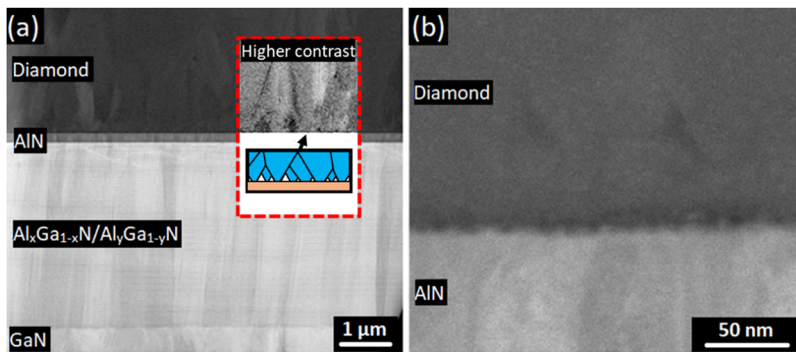


FIG. 5. Cross-sectional STEM showing (a) the III-nitride epitstructure (AlN nucleation, AlGa_N strain relief, and GaN buffer layers) and the diamond, with a higher contrast inset highlighting diamond columnar growth and (b) a close up view of the diamond/AlN interface.

expression. This approximate value lies within the range measured across a membrane by Raman spectroscopy [Fig. 4(b)]. The presence of tensile stress is indicative of a strong bond between the diamond and the III-nitride structure, which can withstand such large stresses. If the III-nitride membrane was delaminated from the diamond, the GaN layer would be more relaxed, which is not observed.

A high-quality diamond/AlN interface is observed in 0.5 mm diameter circular membranes using STEM [Figs. 5(a) and 5(b)], with no voids or cracks visible, confirming the presence of a strong bond. The scale of the interfacial roughness broadly correlates with N-polar AlN surface morphology after Si substrate removal, shown in Fig. 2(d), which seems to have been preserved following diamond growth. At the early stages, heteroepitaxial diamond growth follows the Volmer–Weber mechanism, the three-dimensional growth of diamond islands, until sufficient lateral growth results in film coalescence followed by columnar growth, highlighted in Fig. 5(a).

We note that in the present structure there is a low thermal conductivity AlGa_N strain relief layer between the GaN where transistor current would flow and the diamond. Removing this AlGa_N layer is ultimately important for efficient heat transport between a device channel heat source and the diamond substrate. In this work, we have shown that seeding the AlN layer initiates diamond growth, which is strongly bonded. There is no technological barrier to the incorporation of an AlN “initiation” layer into the GaN buffer close to the device channel,²¹ which can be accessed via the plasma etching methods described previously in combination with highly selective removal of GaN, stopping on the AlN.²² This is the next step to the realization of high power density GaN RF devices,¹ with improved output power and reliability.

In conclusion, cross-sectional STEM and Raman spectroscopy analyses confirm the establishment of a method to strongly bond high quality MPCVD deposited polycrystalline diamonds to N-polar III-nitride membranes formed from GaN-on-Si wafers by selective area substrate removal. The approach obviates the need for wafer bonding and thus provides a route to GaN-on-diamond devices and circuits with improved manufacturability.

The authors would like to acknowledge financial support from the Engineering and Physical Sciences Research Council (EPSRC) under the program Grant GaN-DaME (Grant No. EP/P00945X/1).

DATA AVAILABILITY

The data that support the findings of this study are available from the corresponding author upon reasonable request.

REFERENCES

- J. W. Pomeroy, R. B. Simon, H. Sun, D. Francis, F. Faili, D. J. Twitchen, and M. Kuball, *IEEE Electron Device Lett.* **35**, 1007 (2014).
- H. Sun, R. B. Simon, J. W. Pomeroy, D. Francis, F. Faili, D. J. Twitchen, and M. Kuball, *Appl. Phys. Lett.* **106**, 111906 (2015).
- T. Liu, Y. Kong, L. Wu, H. Guo, J. Zhou, C. Kong, and T. Chen, *IEEE Electron Device Lett.* **38**, 1417 (2017).
- D. Francis, F. Faili, D. Babić, F. Ejeckam, A. Nurmikko, and H. Maris, *Diamond Relat. Mater.* **19**, 229 (2010).
- L. Yates, J. Anderson, X. Gu, C. Lee, T. Bai, M. Mecklenberg, T. Aoki, M. S. Goody, M. Kuball, E. L. Piner, and S. Graham, *ACS Appl. Mater. Interfaces* **10**, 24302 (2018).
- Y. Zhou, J. Anaya, J. W. Pomeroy, H. Sun, X. Gu, A. Xie, E. Beam, M. Becker, T. A. Grotjohn, C. Lee, and M. Kuball, *ACS Appl. Mater. Interfaces* **9**, 34416 (2017).
- T. Gerrer, A. Graff, M. Simon-Najasek, H. Czap, T. Maier, F. Benkhelifa, S. Muller, C. Nebel, P. Waltereit, R. Quay, and V. Cimalla, *Appl. Phys. Lett.* **114**, 252103 (2019).
- T. Gerrer, V. Cimalla, P. Waltereit, S. Muller, F. Benkhelifa, T. Maier, A. Graff, H. Czap, C. Nebel, and R. Quay, in *12th European Microwave Integrated Circuits Conference (EuMIC)* (IEEE, Nuremberg, Germany, 2017), pp. 25–28.
- M. J. Tadjer, T. J. Anderson, M. G. Ancona, P. E. Raad, P. Komarov, T. Bai, J. C. Gallagher, A. D. Koehler, M. S. Goorsky, D. A. Francis, K. D. Hobart, and F. J. Kub, *IEEE Electron Device Lett.* **40**, 881 (2019).
- C. Q. Chen, J. P. Zhang, M. E. Gaevski, H. M. Wang, W. H. Sun, R. S. Q. Fareed, J. W. Yang, and M. A. Khan, *Appl. Phys. Lett.* **81**, 4961 (2002).
- F. Laerme, A. Schilp, K. Funk, and M. Offenberger, in *Technical Digest. IEEE International MEMS 99 Conference. Twelfth IEEE International Conference on Micro Electro Mechanical Systems* (IEEE, Orlando, FL, USA, 1999), pp. 211–216.
- S. Mandal, C. Yuan, F. Massabuau, J. W. Pomeroy, J. Cuenca, H. Bland, E. Thomas, D. Wallis, T. Batten, D. Morgan, R. Oliver, M. Kuball, and O. A. Williams, *ACS Appl. Mater. Interfaces* **11**, 40826 (2019).
- Y. Hayashi, R. Katayama, T. Akiyama, T. Ito, and H. Miyake, *Appl. Phys. Express* **11**, 031003 (2018).
- S. Praver and R. J. Nemanich, *Philos. Trans. R. Soc. London, Ser. A* **362**, 2537 (2004).
- R. J. Atkinson, W. J. Winkworth, and G. M. Norris, *Behaviour of Skin Fatigue Cracks at the Corners of Windows in a Comet I Fuselage* (H.M. Stationary Office, London, 1962), p. 4.
- F. Demangeot, J. Frandon, P. Baules, F. Natali, F. Semond, and J. Massies, *Phys. Rev. B* **69**, 155215 (2004).
- C.-L. Hsiao, L.-W. Tu, T.-W. Chi, M. Chen, T.-F. Young, C.-T. Chia, and Y.-M. Chang, *Appl. Phys. Lett.* **90**, 043102 (2007).

¹⁸R. Nowak, M. Pessa, M. Sukanuma, M. Leszczynski, I. Grzegory, S. Porowski, and F. Yoshida, *Appl. Phys. Lett.* **75**, 2070 (1999).

¹⁹A. U. Sheleg and V. A. Savastenko, *Vesti Akad. Navuk BSSR, Ser. Fiz.-Mat. Navuk* **3**, 126 (1976).

²⁰M. J. Edwards, C. R. Bowen, D. W. E. Allsopp, and A. C. E. Dent, *J. Phys. D: Appl. Phys.* **43**, 385502 (2010).

²¹M. Kuball, J. W. Pomeroy, M. Uren, and O. A. A. Williams, "A semiconductor on diamond substrate, precursor for use in preparing a semiconductor on diamond substrate, and methods for making the same," GB patent: GB 1814192.9 (2019).

²²S. A. Smith, C. A. Wolden, M. D. Bremser, A. D. Hanser, and R. F. Davis, *Appl. Phys. Lett.* **71**, 3631 (1997).